

Decoherence from Long-Range Forces in Atom Interferometry

Jonathan Kunjummen,^{1,*} Daniel Carney,² and Jacob M. Taylor¹

¹*Joint Quantum Institute/Joint Center for Quantum Information and Computer Science, University of Maryland, College Park/National Institute of Standards and Technology, Gaithersburg, MD, USA*

²*Physics Division, Lawrence Berkeley National Laboratory, Berkeley, CA, USA*

(Dated: May 9, 2022)

Abstract

Atom interferometers provide a powerful means of realizing quantum coherent systems with increasingly macroscopic extent in space and time. These systems provide an opportunity for a variety of novel tests of fundamental physics, including ultralight dark matter searches and tests of modifications of gravity, using long drop times and microgravity environments. However, as experiments operate with longer periods of free fall and become sensitive to smaller background effects, key questions start to emerge about the fundamental limits to future atom interferometry experiments. We study the effects on atomic coherence from hard-to-screen backgrounds due to baths of ambient particles with long-range forces, such as gravitating baths and charged cosmic rays. Our approach – working in the Heisenberg picture for the atomic motion – makes proper inclusion of the experimental apparatus feasible and clearly shows how to handle long-range forces and preferred frame ambiguities. We find that these potential backgrounds are likely negligible for the next generation of interferometers, as aggressive estimates for the gravitational decoherence from a background bath of dark matter particles gives a decoherence timescale on the order of years.

* jkunjumm@umd.edu

CONTENTS

I. Introduction	2
II. Background Model	4
III. Prototypical Experiment	6
A. Case Study: Uniform Acceleration	11
B. Distant Sector	12
IV. Relationship to Collisional Brownian Motion	16
V. Collision Cone Sector	18
VI. Tuning the Sensor: the Choice of Atom-Laser Distance	22
VII. Cosmic Rays	24
VIII. Outlook	26
IX. Acknowledgments	26
A. Time Dependence in the Distant Sector	26
References	28

I. INTRODUCTION

Atom interferometers (AIs) are useful both in enabling new measurements and in providing better understandings of key concepts in quantum mechanics and its intersection with relativity [1]. Based on the concept of particle interference, the simplicity of the atom interferometer in principle provides key ways of testing the connection between path integrals and Hamiltonian quantum dynamics [2], explorations of the concept of ‘which-way’ information [3–7], and considerations of the distinctions between interferometry in a Galilean frame and in a fully general relativistic frame [8]. At the same time, AIs are exquisitely sensitive to small variations in local accelerations and rates of rotation. Early work showcased measurements of the tides [9] and seismic backgrounds [10, 11] while more recent developments include precision geodesy and gravity gradient detection [12–14]. In the next decade, AIs will see increasing use in searches for new fundamental physics, including low-frequency gravitational waves and ultralight dark matter [15–19] and tests of modifications of gravity

[20, 21].

Typically, the dominant background noise in AI systems is assumed to be a combination of different terrestrial sources, due to local gas particles in the (imperfect) vacuum, or due to laser-related noise sources [22]. Here, we instead consider the effect of both distant and close gravitational sources that may be due, e.g., to particulate models of dark matter or more distant, heavier astrophysical objects [23]. Due to the unscreened, long-range nature of the gravitational coupling, this type of background is unavoidable for AIs. By examining this potential signal, we can put bounds on the fundamental performance limits of AIs in both earth-based and space-based settings, conditional on a variety of models for background particles. This work also contributes to the study of irreducible gravitational backgrounds that optomechanical experiments probing quantum macroscopicity and gravity from quantum objects will face [24–40].

In addition to practical reasons for wanting to characterize this background, the case of gravitational noise is conceptually interesting, first because of equivalence principle considerations and second because of the infinite scattering cross section of the $1/r$ potential. Typically, to account for background particles one need only include their interaction with the atom [41–43]. Things become more complicated when we consider gravitational interactions, however, since for instance we know that a constant gravitational field acts on all components of an experiment so as to be undetectable in freefall. To capture this in the formalism describing the experiment, one must account for the effect of the gravitational field on the control system, not just the atom [8, 27, 44]. A central result of our work is to provide a clean conceptual framework that treats the AI apparatus and the atoms themselves on an equal footing, thus properly treating issues involving the equivalence principle, which is an essential first step for taking AI into the space-based regime. Our approach also addresses a conceptual issue which occurs when trying to apply traditional Brownian motion calculations [41–43] when the bath has a long-range, unscreened coupling to the apparatus. As we will explain, the naive prediction of an infinite decoherence rate for a $1/r$ potential is fixed by including the infrared cutoff set by the spatial extent of the experimental apparatus [45, 46]. As we show below, the effect is likely to be small for models of dark matter under current consideration, but this study opens the door to exploring dark matter or other particulate detection using AIs when the interaction is not (only) gravitational, and to this end we consider interactions with cosmic ray particles at the end of the paper.

The paper is organized as follows. In Section II we set up the model for an atom interferometer in the presence of background particles that interact with a long-range force with both the atoms and the experimental apparatus. In Section III we set up the formalism describing our atom interferometry experiment, and show how the effects of a constant, global acceleration on the atom and on the control system cancel out, in accordance with the Equivalence Principle. This allows us to we analyze the effect of a cloud of distant bath particles on the experiment. In Section IV, we discuss the relationship between this calculation and the standard quantum Brownian motion framework. In Section V we calculate the effect of nearby bath particles, in particular considering atom interferometers as dark matter detectors. In Section VI we discuss the usefulness of tuning the atom-laser distance to change sensitivity of the experiment to the gravitational background. In Section VII we consider atom interferometers as impulse detectors for more general forces, examining the case of a passing charged cosmic ray particle. Finally, we summarize our results and consider future work in Section VIII.

II. BACKGROUND MODEL

In this paper we consider a simplified atom interferometer in microgravity, as shown in Fig. 1a, where the dominant gravitational acceleration is from a cloud of N identical background particles of mass m_b interacting with the setup via gravity. This model is relevant to the behavior of proposed atom interferometers in space, where the free evolution times are not limited by the need to construct a long drop tower [15]. We restrict ourselves to a highly simplified atom interferometry model, in which atomic motion takes place along only one axis and there is only a single control laser, in order to focus on the effect of gravitational noise. Specifically, as described below, this interferometer is sensitive to local accelerations. A uniform acceleration introduces no relative motion between the control apparatus and the atom, and is therefore unobservable. Gravitational noise results, then, when an unknown background gravitational field introduces relative motion between any of three parts of the experiment: the control system and either of the paths taken by the atom in superposition. To model this carefully, and in contrast to prior work, we explicitly include in our analysis the motion of the laser which implements the beamsplitter and mirror operations.

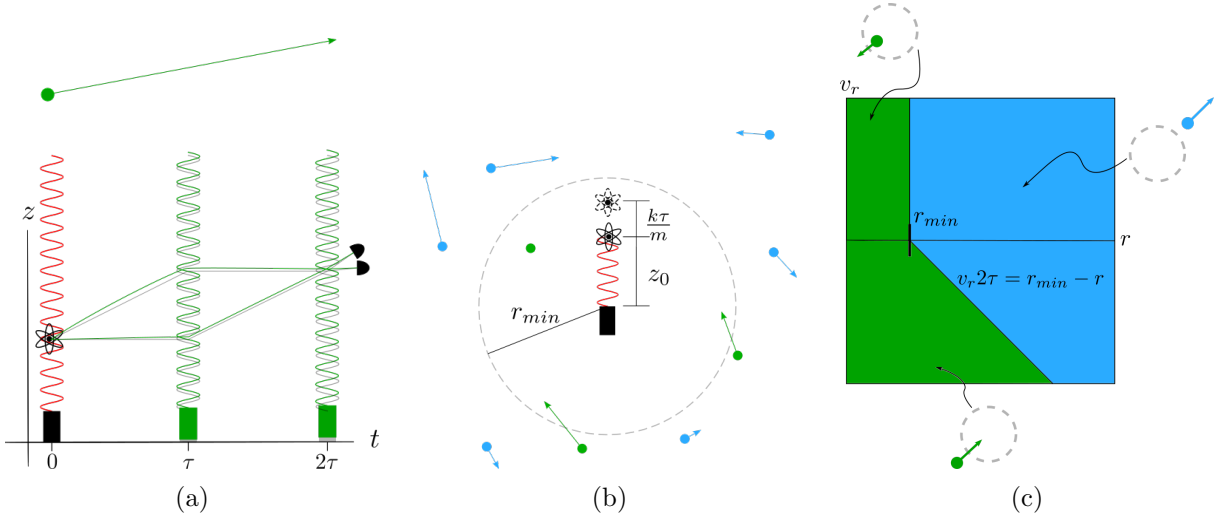


FIG. 1. Schematic of atom interferometry taking place in the presence of background particles. a) Schematic of atom interferometry. The atom begins in the ground state and then undergoes a $\frac{\pi}{2} - \pi - \frac{\pi}{2}$ pulse sequence, after which the internal state is measured. A passing bath particle leads to distortions of the laser and atom trajectories. b) Particles which remain outside r_{min} through the whole experiment (light blue) source a gravitational potential varying slowly across the spatial extent of the experiment. Those which start or drift inside r_{min} are in the collision cone (green). The atom starts a distance z_0 from the laser, and is put into a superposition of paths with maximum separation $\hbar k\tau/m$. c) Division of phase space into distant sector (blue) and collision cone (green). This is a cross section of the full phase space at zero angular velocity and arbitrary angular coordinates. The collision cone includes particles which begin inside the cutoff radius r_{min} , as well as those which begin outside but have an inward velocity large enough to bring them within r_{min} by time 2τ .

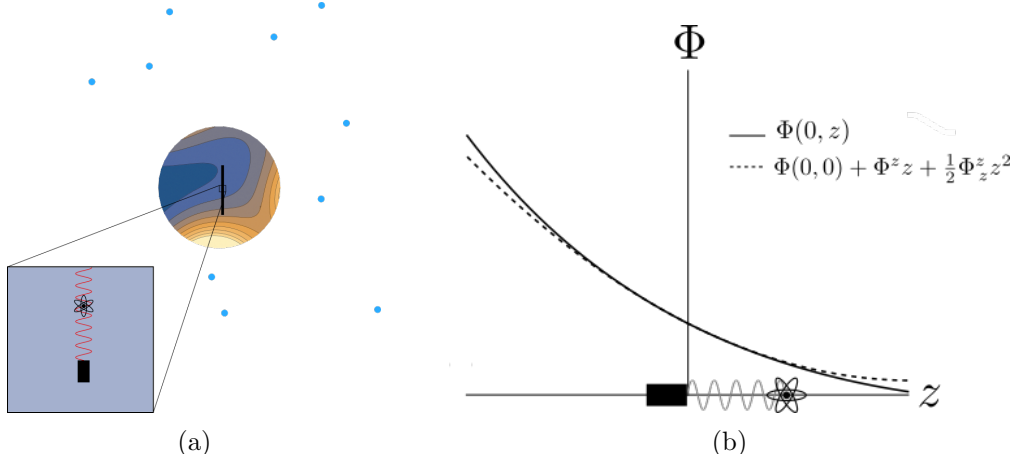


FIG. 2. a) Contour plot in two dimensions of the gravitational potential sourced by particles outside the cutoff radius r_{min} . b) Comparison of the actual potential and the second order multipole approximation to it near the origin along the one dimensional slice shown in part a).

For simplicity, we ignore interactions between the bath particles, and assume that at the beginning of the experiment they are statistically distributed according to a free particle Boltzmann distribution with some effective temperature T

$$P(\mathbf{r}_b, \mathbf{v}_b) = \frac{1}{V} \left(\frac{m_b}{2\pi k_B T} \right)^{-\frac{3}{2}} \exp\left\{-\frac{m_b \mathbf{v}_b^2}{2k_B T}\right\} \quad (1)$$

where k_B is Boltzmann's constant, and V is the volume of all space. We will eventually take the large N and large V limit, with finite number density $n_0 \equiv N/V$.

If a particle is much farther from the setup than the atom-laser distance, then the potential it produces near the experiment can be approximated with a multipole expansion whose first order terms constitute a global acceleration. We therefore divide the phase space of a bath particle into two sectors by choosing some cutoff radius r_{min} much larger than the spatial extent of the experiment, and then separating the part of phase space which will stay outside this radius for the entire duration of the experiment from the part which is inside r_{min} during some or all of the experiment. This division, which depends on the experimental runtime, is illustrated graphically in Fig. 1c. We will examine the effect of each of these phase sectors on an atom interferometry experiment in turn. In order to calculate what the effect of this is on atom interferometry, we need to define the experimental procedure in detail.

III. PROTOTYPICAL EXPERIMENT

We analyze a pedagogical model of atom interferometry to focus on the effects of gravitational noise. Specifically, we consider an experiment with two components, a laser of mass M_{laser} and position $\mathbf{R}_{\text{laser}}$ and a two-level atom of mass m_a and position $\hat{\mathbf{r}}$. The laser produces light with wavevector $\mathbf{k} = k \mathbf{e}_3$ which we treat classically. We emphasize that for the purposes of this calculation, we neglect the spatial distribution and relative motion of different components of the laser system. Assuming that all effects leading to phase shifts in the laser light are captured by a single gravitational potential acting on the laser center of mass, which we write as $-GM_{\text{laser}}\Phi(\mathbf{R}_{\text{laser}})$ with G the gravitational constant, the evolution

of the laser is governed by the classical equations of motion

$$\dot{\mathbf{R}}_{\text{laser}} = \mathbf{P}_{\text{laser}}/M_{\text{laser}} \quad (2)$$

$$\dot{\mathbf{P}}_{\text{laser}} = GM_{\text{laser}}\nabla\Phi(\mathbf{R}_{\text{laser}}). \quad (3)$$

The evolution of the atom degrees of freedom is governed by the following Hamiltonian, making the rotating wave approximation and moving to the interaction picture with respect to the atom's internal degree of freedom:

$$\hat{H} = \hat{H}_{\text{atom}} + \hat{H}_{\text{int}} \quad (4)$$

$$\hat{H}_{\text{atom}} = \frac{\hat{\mathbf{p}}^2}{2m_a} - Gm_a\hat{\Phi}(\hat{\mathbf{r}}) - \frac{\hbar\Delta}{2}\hat{\sigma}_z \quad (5)$$

$$\hat{H}_{\text{int}} = \frac{\hbar\Omega(t)}{2} e^{ik(\hat{z} - Z_{\text{laser}}(t)) - i\Delta t} \hat{\sigma}_+ + \text{h.c.}, \quad \hat{\sigma}_+ = \hat{\sigma}_-^\dagger = |\uparrow\rangle\langle\downarrow|, \quad (6)$$

where $\Omega(t)$ is the slowly varying Rabi frequency and h.c. stands for Hermitian conjugate. We stress that the gravitational potential after factoring out the mass, which we denote Φ , has the same functional form for both the atom and the laser, which will lead to the noise cancellations associated with the equivalence principle. From now on we work on resonance, setting $\Delta = 0$ in what follows.

Notice we make the approximation that the magnitude of the coupling between the atom and the laser field depends only on time, not on the location of the atom in space. We also ignore time retardation effects in the location of the laser seen by the atom. These approximations are valid if the laser beam is much broader than the atom cloud at all times, and if the time it takes light to travel from the laser to the atom is much faster than the timescale on which the laser amplitude changes.

To implement our experimental protocol, for simplicity we take the pulse envelope $\Omega(t)$ to be a sequence of delta functions giving a three pulse sequence

$$\Omega(t) = \frac{\pi}{2}\delta(t) + e^{-i\theta_0/2}\pi\delta(t - \tau) + \frac{\pi}{2}\delta(t - 2\tau), \quad (7)$$

where θ_0 is a tunable phase set by the experimenter and τ is the time between pulses. We can approximate the pulses as delta functions as long as the pulses are much faster than the dynamics of the laser and atom position. After the pulse at time 2τ we then measure the

state of the atom in the \uparrow, \downarrow basis.

We focus on making measurements of the internal state of the atom, using a spinor notation so that $|\chi\rangle$ denotes the full spinor state, whereas $|\psi\rangle$ denotes a state in real space only. In this way we write

$$|\chi\rangle = |\psi_\uparrow\rangle \otimes |\uparrow\rangle + |\psi_\downarrow\rangle \otimes |\downarrow\rangle = \begin{pmatrix} |\psi_\uparrow\rangle \\ |\psi_\downarrow\rangle \end{pmatrix} \quad (8)$$

with normalization condition,

$$1 = \langle \chi | \chi \rangle = \langle \psi_\uparrow | \psi_\uparrow \rangle + \langle \psi_\downarrow | \psi_\downarrow \rangle = \int d^3\mathbf{r} \left(|\psi_\uparrow(\mathbf{r})|^2 + |\psi_\downarrow(\mathbf{r})|^2 \right) \quad (9)$$

so that $|\psi_\uparrow(\mathbf{r})|^2$ gives the probability density for finding the atom in the excited state at \mathbf{r} and likewise $|\psi_\downarrow(\mathbf{r})|^2$ for the ground state. Generally, we will assume measurements do not resolve atomic position and thus we only have access to the probabilities after integration

$$\text{Prob}(\uparrow) = \int d^3\mathbf{r} |\psi_\uparrow(\mathbf{r})|^2 \quad (10)$$

and likewise for spin down.

To calculate the experimental signal, we work in terms of the unitary operator generated by the Hamiltonian. This approach is complementary to the path integral method, used widely to describe atom interferometers [47]. Our current approach is convenient, however, in that it easily incorporates laser motion, failure of the two paths to interfere, and (as will be shown in Section V) impulses from nearby bath particles which perturb the atomic trajectories significantly. Given the pulse sequence of Eqn. 7, the solution to the Schrodinger Equation can be expressed in terms of a few unitary operators, first the unitary corresponding to free evolution between pulses

$$U_{\text{atom}}(t_1, t_2) = \mathcal{T} \exp \left\{ -i \int_{t_1}^{t_2} \frac{dt H_{\text{atom}}(t)}{\hbar} \right\} \quad (11)$$

and next the unitaries corresponding to the instantaneous $\pi/2$ and π pulses (we neglect the

effect of gravity during the pulses)

$$U_{\pi/2}(t) \equiv \exp\left\{-i\left(\frac{\pi}{4}e^{ik(\hat{z}-Z_{\text{laser}}(t))}\sigma_+ + \text{h.c.}\right)\right\} = \frac{1}{\sqrt{2}}\mathbb{1} - \frac{i}{\sqrt{2}}\left(e^{ik(\hat{z}-Z_{\text{laser}}(t))}\sigma_+ + \text{h.c.}\right) \quad (12)$$

$$U_\pi(t) \equiv \exp\left\{-i\left(\frac{\pi}{2}e^{i(k(\hat{z}-Z_{\text{laser}}(t))-\theta_0/2)}\sigma_+ + \text{h.c.}\right)\right\} = -\frac{i}{\sqrt{2}}\left(e^{i(k(\hat{z}-Z_{\text{laser}}(t))-\theta_0/2)}\sigma_+ + \text{h.c.}\right) \quad (13)$$

where $Z_{\text{laser}}(t)$ is of course evolved by the classical equations of motion, Eqns. 2, 3.

The spinor state at the end of the protocol is

$$|\chi(2\tau)\rangle = U_{\pi/2}(2\tau) U_{\text{atom}}(\tau, 2\tau) U_\pi(\tau) U_{\text{atom}}(0, \tau) U_{\pi/2}(0) |\chi(0)\rangle \quad (14)$$

So, taking the initial atomic state to be entirely in the ground state with spatial wavefunction $|\psi_{\downarrow, t=0}\rangle$

$$|\chi(0)\rangle = \begin{pmatrix} 0 \\ |\psi_{\downarrow, t=0}\rangle \end{pmatrix} \quad (15)$$

we get the final spinor state

$$|\chi(2\tau)\rangle = \frac{1}{2} \begin{pmatrix} ie^{ik(\hat{z}-Z_{\text{laser}}(2\tau))} (U^t - U^b) |\psi_{\downarrow, t=0}\rangle \\ -(U^t + U^b) |\psi_{\downarrow, t=0}\rangle \end{pmatrix}, \quad (16)$$

where we have defined the operators

$$U^t = e^{i\frac{\theta_0}{2}} U_{\text{atom}}(\tau, 2\tau) e^{-ik(\hat{z}-Z_{\text{laser}}(\tau))} U_{\text{atom}}(0, \tau) e^{ik\hat{z}} \quad (17)$$

$$U^b = e^{-i\frac{\theta_0}{2}} e^{-ik(\hat{z}-Z_{\text{laser}}(2\tau))} U_{\text{atom}}(\tau, 2\tau) e^{ik(\hat{z}-Z_{\text{laser}}(\tau))} U_{\text{atom}}(0, \tau) \quad (18)$$

which act only on the center of mass degree of freedom.

The two unitaries U^t, U^b correspond to the two arms of the interferometer as shown in Fig. 1a [48]. To provide some intuition, there are two ways an atom can end up in the ground state. The ground state contribution from the top arm (described by U^t) is excited by the first $\pi/2$ pulse, de-excited by the π pulse, and left unchanged by the second $\pi/2$ pulse. The contribution from the bottom arm (described by U^b) corresponds to the component unchanged by the first $\pi/2$ pulse, excited by the π pulse, and de-excited by the last $\pi/2$ pulse. These two contribution follow different real space paths, as demonstrated

in the figure. These same operators U^t, U^b are summed to calculate the final excited state wavefunction in the top entry of Eqn. 16, but they are multiplied by a final momentum kick—as the excited state still carries the photon momentum—and summed with a different relative phase as is required to conserve probability.

We can calculate the diagonal entries of the spin density matrix, i.e. the populations of the ground and excited state, at the end of the experiment

$$\rho_{\downarrow\downarrow} = 1 - \rho_{\uparrow\uparrow} = \frac{1}{2} + \frac{1}{2} \operatorname{Re} \langle \psi_{\downarrow, t=0} | (U^b)^\dagger U^t | \psi_{\downarrow, t=0} \rangle \quad (19)$$

and as expected, if the spatial wavefunctions at the end of the two arms do not overlap, i.e $\langle (U^b)^\dagger U^t \rangle = 0$, the contributions from the two arms cannot interfere, and both states will be equally populated. If there is no external potential, then $(U^b)^\dagger U^t = e^{i\theta_0}$ and the output population is simply

$$\rho_{\downarrow\downarrow}^{\text{free}} = \frac{1}{2} + \frac{1}{2} \cos \theta_0. \quad (20)$$

In this case, by tuning θ_0 , we can tune the final population all the way from entirely ground state to entirely excited state.

Gravitational noise changes the overlap between the two paths, and can cause both phase shifts in the cosine term and an overall reduction in contrast. We will quantify decoherence from gravitational noise by how it decreases our ability to tune the final population via θ_0 . We rearrange the terms in the path-specific unitaries to get

$$U^t = e^{i\frac{\theta_0}{2}} U_{\text{atom}}(0, 2\tau) e^{-ik(\hat{z}(\tau) - Z_{\text{laser}}(\tau))} e^{ik\hat{z}} \quad (21)$$

$$U^b = e^{-i\frac{\theta_0}{2}} U_{\text{atom}}(0, 2\tau) e^{-ik(\hat{z}(2\tau) - Z_{\text{laser}}(2\tau))} e^{ik(\hat{z}(\tau) - Z_{\text{laser}}(\tau))} \quad (22)$$

written in terms of the interaction picture position operator

$$\hat{z} \rightarrow \hat{z}(t) = \left(U_{\text{atom}}(0, t) \right)^\dagger \hat{z} U_{\text{atom}}(0, t) \quad (23)$$

we can then rewrite the overlap factor in the interaction picture

$$\begin{aligned} (U^b)^\dagger U^t &= (U_{\text{atom}}^\dagger(0, 2\tau) U^b)^\dagger U_{\text{atom}}^\dagger(0, 2\tau) U^t \\ &= e^{i\theta_0} \left(e^{-ik(\hat{z}(2\tau) - Z_{\text{laser}}(2\tau))} e^{ik(\hat{z}(\tau) - Z_{\text{laser}}(\tau))} \right)^\dagger e^{-ik(\hat{z}(\tau) - Z_{\text{laser}}(\tau))} e^{ik\hat{z}} \end{aligned} \quad (24)$$

From this we see that the output of the atom interferometer depends solely on the evolution of the position operator $\hat{z}(t)$ relative to the laser position. Thus, shared acceleration is unobservable in this setup, as expected from the equivalence principle.

A. Case Study: Uniform Acceleration

To illustrate the importance of including the effect of gravity on the control system, before going further with our model of the gravitational noise background we consider an experiment subject to global acceleration g , i.e.

$$G \Phi(\mathbf{R}_{\text{laser}}) = g Z_{\text{laser}} \quad (25)$$

and an analogous expression holds for the atom with the appropriate quantities promoted to operators. The classical and Heisenberg equations of motion in this case can be solved exactly to give the evolution of the laser position and atom center of mass

$$Z_{\text{laser}}(t) = Z_{\text{laser}}(0) + \dot{Z}_{\text{laser}}(0)t + \frac{1}{2}gt^2 \quad (26)$$

$$\hat{z}(t) = \hat{z} + \hat{p}_z t/m_a + \frac{1}{2}gt^2. \quad (27)$$

We will always choose our coordinate system so that the laser starts out at rest at the origin, $Z_{\text{laser}}(0), \dot{Z}_{\text{laser}}(0) = 0$. We subsequently can evaluate Eqn. 24 with

$$\hat{z}(t) - Z_{\text{laser}}(t) = \hat{z} + \hat{p}_z t/m_a. \quad (28)$$

But of course, this is how the relative displacement would evolve if the apparatus was floating in free space. The output spin down population is again given by Eqn. 20 with no dependence on the global acceleration g , so indeed the equivalence principle is satisfied. We

now have the tools in place to explore our gravitational noise model. We first examine the distant sector.

B. Distant Sector

We now analyze the bath model introduced earlier, which gives rise to a gravitational potential

$$G\hat{\Phi}(\hat{\mathbf{r}}) \equiv G m_b \sum_{n=1}^N \frac{1}{|\mathbf{r}_{b_n} - \hat{\mathbf{r}}|}.$$

Bath particles in the distant sector produce a gravitational potential near the experiment that can be approximated with a multipole expansion as shown in Figs. 2a-2b,

$$\hat{\Phi}(\hat{\mathbf{r}}) \approx \Phi(\mathbf{0}) + \Phi^i \hat{r}_i + \frac{1}{2} \hat{r}_i \Phi^i_j \hat{r}^j \quad (29)$$

where repeated indices are summed over the three spatial axes, but as this is a nonrelativistic calculation there is no distinction between covariant and contravariant vectors. We have kept the terms leading to a global acceleration

$$\Phi^i \equiv \frac{\partial}{\partial \hat{r}_i} \hat{\Phi}(\hat{\mathbf{r}}) \Big|_{\hat{\mathbf{r}}=\mathbf{0}} \quad (30)$$

and the quadratic terms

$$\Phi^i_j \equiv \frac{\partial^2}{\partial \hat{r}_i \partial \hat{r}_j} \hat{\Phi}(\hat{\mathbf{r}}) \Big|_{\hat{\mathbf{r}}=\mathbf{0}}. \quad (31)$$

We emphasize, too, that although $\hat{\Phi}(\hat{\mathbf{r}})$ is an operator, the coefficients Φ^i , Φ^i_j are real numbers.

We can calculate the explicit form of the quadratic coefficients Φ^i_j

$$\Phi_z^z \equiv m_b \sum_{n=1}^N \frac{-r_{b_n}^2 + 3z_{b_n}^2}{r_{b_n}^5} \quad (32)$$

$$\Phi_y^z \equiv m_b \sum_{n=1}^N \frac{3z_{b_n} y_{b_n}}{r_{b_n}^5}, \quad (33)$$

with rotational symmetry fixing all other components given these two. Following the argument in the uniform acceleration case study, we note that the Φ^i terms are not observable as they produce identical displacement of the laser and the atom, therefore we do not bother to list them explicitly. Because we assume the different bath particles are distributed independently, any function $f(\Phi_j^i)$ has expectation value

$$\langle f(\Phi_j^i) \rangle = \frac{1}{V^N} \left(\frac{m_b}{2\pi k_B T} \right)^{\frac{3N}{2}} \iint_{\text{distant}} d^{3N}\{\mathbf{r}_{b_n}\} d^{3N}\{\mathbf{v}_{b_n}\} \exp\left\{-\frac{m_b}{2k_B T} \sum_n \mathbf{v}_{b_n}^2\right\} f(\Phi_j^i(\{\mathbf{r}_{b_n}\}, \{\mathbf{v}_{b_n}\}, t)), \quad (34)$$

where the subscript on the integrals indicates that we are averaging over the distant phase space sector as shown in Fig. 1c.

In general the Φ_j^i are time dependent because of the motion of the bath particles, but in this section we will assume the zero temperature limit for simplicity. We calculate the lowest order correction from bath particle motion in Appendix A. In the zero temperature case, all background particles are at rest, and the collision cone particles are simply those that begin inside the cutoff radius. For any finite thermal bath velocity v_β , the zero temperature approximation gives increasingly accurate behavior for the distant sector (though not for the collision cone) as we take $r_{\min} \rightarrow \infty$, because changes in the gravitational field near the origin over the course of the experiment are suppressed by $v_\beta \tau / r_{\min}$. We can drop the velocity averaging in the zero temperature limit and simply average over possible bath particle locations. If the average volume per bath particle is much smaller than the excluded volume, $n_0 r_{\min}^3 \gg 1$, the components of Φ_j^i are approximately Gaussian distributed with zero mean and variance

$$\langle (G \Phi_j^i)^2 \rangle = \frac{4\pi}{3} \frac{3 + \delta_{ij}}{5} \xi^2, \quad \xi^2 \equiv \frac{(Gm_b)^2 n_0}{r_{\min}^3}. \quad (35)$$

In our units, ξ^2 has dimension [1/time⁴]. The trace of the matrix of quadratic terms is identically zero, so some of its components are correlated. We will skip over this subtlety, however, as only an uncorrelated set of components ends up contributing in the lowest order correction to the flat space behavior.

As in the global acceleration case, we solve the Heisenberg and classical equations of

motion for $\hat{z}, Z_{\text{laser}}$ respectively to calculate the evolution of the laser-atom separation

$$\hat{z}(t) - Z_{\text{laser}}(t) \approx \hat{z} + t \frac{\hat{p}_z}{m_a} + \frac{t^2}{2!} G \Phi_j^z \hat{r}^j + \frac{t^3}{3!} G \Phi_j^z \frac{\hat{p}^j}{m_a} + \frac{t^4}{4!} G^2 \Phi_j^z \Phi_k^j \hat{r}^j + \frac{t^5}{5!} G^2 \Phi_j^z \Phi_k^j \frac{\hat{p}^k}{m_a}, \quad (36)$$

where we have dropped terms past second order in the gravitational potential, assuming $\xi^2 \tau^4 \ll 1$. At the end of the protocol, for a fixed bath configuration, we get a ground state population

$$\rho_{\downarrow\downarrow} = \frac{1}{2} + \frac{1}{2} \text{Re} \langle \psi_{\downarrow}(0) | \exp\{i(\hat{\Theta} + \theta_0)\} | \psi_{\downarrow}(0) \rangle \quad (37)$$

$$\begin{aligned} \hat{\Theta} \equiv & \left(\frac{G \Phi_z^z \tau^2}{2} + \frac{G^2 \Phi_j^z \Phi_z^j \tau^4}{8} \right) \frac{\hbar k^2 \tau}{m_a} + k \left(G \Phi_i^z \tau^2 + \frac{7}{12} G^2 \Phi_j^z \Phi_i^j \tau^4 \right) \hat{r}^i \\ & + \frac{k \tau}{m_a} \left(G \Phi_i^z \tau^2 + \frac{1}{4} G^2 \Phi_j^z \Phi_i^j \tau^4 \right) \hat{p}^i + \mathcal{O}(\xi^3 \tau^6). \end{aligned} \quad (38)$$

The operator $e^{i\hat{\Theta}}$ is a phase space displacement, and depends on the bath configuration.

We take for our initial real space wavefunction a Gaussian wavepacket with isotropic width σ , centered in phase space at position $\mathbf{z}_0 = z_0 \mathbf{e}_3$ and at zero momentum. Denoting our initial state $|\mathbf{z}_0, 0\rangle$, we find

$$\langle \mathbf{z}_0, 0 | e^{i\hat{\Theta}} | \mathbf{z}_0, 0 \rangle \approx \exp\{ik(z_0 + \frac{\hbar k \tau}{2m_a}) \tau^2 G \Phi_z^z + (i \frac{7kz_0}{12} + i \frac{\hbar k^2 \tau}{8m_a} - \frac{k^2 \sigma^2}{2} - \frac{\hbar^2 k^2 \tau^2}{8m_a^2 \sigma^2}) \tau^4 G^2 \Phi_j^z \Phi_z^j\}, \quad (39)$$

again keeping only terms up to second order in the interaction, which requires the additional assumption $k^2 \sigma^2 \xi^2 \tau^4 \ll 1$. The dominant term in this expression is

$$\mathcal{D} \equiv \exp\{ikd\tau^2 G \Phi_z^z\}, \quad (40)$$

a phase shift linear in Φ_z^z and in the quantity $d \equiv z_0 + \hbar k \tau / 2m_a$, the distance between the laser and the center of atomic motion. We can think of this as setting an effective dipole moment for the interferometer's response to gravity. Following this there is another phase shift quadratic in Φ , and two inherent decoherence terms set by the nonzero width in phase space of the atomic wavepacket. The sum of these last two terms has a minimum size set

by the standard quantum limit at $\sigma^2 = \hbar\tau/2m_a$.

At this order, since we are working in the regime where Φ_j^z are Gaussian distributed according to Eqn. 35, we can easily trace out the bath as well. We get the following result for the ground state population after averaging over bath configurations, accurate to order $\xi^2\tau^4$:

$$\rho_{\downarrow\downarrow} = \frac{1}{2} + \frac{1}{2} \frac{\exp\{-\frac{8\pi}{15}k^2d^2\xi^2\tau^4\}}{\sqrt{\prod_{j \in \{x,y,z\}} \left(1 + \frac{4\pi}{3}\frac{3+\delta_{z,j}}{5}(k^2\sigma^2 + \frac{\hbar^2k^2\tau^2}{4m_a^2\sigma^2})\xi^2\tau^4\right)}} \cos\left(\theta_0 + \frac{4\pi}{3}k\left(\frac{7}{6}z_0 + \frac{\hbar k\tau}{4m_a}\right)\xi^2\tau^4\right), \quad (41)$$

where we fix the branch of the square roots in Eqn. 41 by demanding that they continuously go to unity as $\tau \rightarrow 0$. Since the real part of the argument is always positive, this eliminates any ambiguity. Tracing the different terms in Eqn. 39 through the general formula for a Gaussian function integrated against a Gaussian probability distribution, we see that the linear in Φ phase shift and the inherent decoherence terms lead to a reduction in overall contrast after averaging over bath configurations, while the phase shift quadratic in Φ actually leads to an average phase shift in the interferometer, to order $\xi^2\tau^4$.

Usually $z_0 \gg \sigma$, so the factor of $\exp\{-\frac{8\pi}{15}k^2d^2\xi^2\tau^4\}$ provides most of the decoherence. From the dependence on the effective dipole moment we see explicitly how increasing the spatial extent of the experiment increases its sensitivity to effects from finite spacetime curvature, as is familiar from discussions of Einstein's elevator. We also see that the atom-laser separation and the maximum atom path separation both play a role in determining the sensitivity to gravitational noise.

We now plug in some typical parameters to get some quantitative understanding of the decoherence behavior. Looking at the dominant contribution to decoherence in Eqn. 41 mentioned above, we see that $t_{decoherence} \equiv (k^2d^2\xi^2)^{-1/4}$ sets a characteristic decoherence timescale. To get an order of magnitude estimate of this timescale, we take r_{min} to be comparable to d . Let us consider dark matter providing the background noise. Since the local mass density of dark matter is fixed by observation (at $m_b n_0 \approx 5 \times 10^{-25}$ g/cm³), the decoherence timescale decreases as we consider increasingly massive dark matter candidates. Taking an optical wavelength of 780 nm and a large dark matter mass of the Planck mass,

m_{pl} , to get an optimistic estimate of the decoherence timescale, we get

$$t_{\text{decoherence}} \approx 10 \text{ years} \left(\frac{m_{\text{pl}}}{m_b} \right)^{\frac{1}{4}} \left(\frac{5 \times 10^{-25} \text{ g/cm}^3}{m_b n_0} \right)^{\frac{1}{4}} \left(\frac{d}{1 \text{ m}} \right)^{\frac{1}{4}} \quad (42)$$

which is clearly unobservable in the near term. Note, too, that in an experiment this long, several of the assumptions that went into the calculation would be violated. Note also that the τ^4 behavior of the exponent in Eqn. 41 makes it very difficult to see decoherence for experiments with duration much shorter than the characteristic decoherence time.

IV. RELATIONSHIP TO COLLISIONAL BROWNIAN MOTION

As discussed in the introduction, dephasing from random baths of background particle collisions with a superposed mass is usually treated through a Brownian motion approach [41–43]. There, the assumption is usually made that the superposed particle is sufficiently heavy that we can ignore changes to its kinetic energy from the scattering, i.e. in the limit $m_a \ll m_b$. The decoherence rate Γ for an object held in a superposition of two locations with separation Δx is then given by the following integral over q , the incoming bath particle momentum:

$$\Gamma = n \int_0^\infty dq f(q, T) \frac{q}{m_b} \sigma(q), \quad (43)$$

in the limit that superposition scale is much larger than the typical bath particle de Broglie wavelength, $\Delta x \sqrt{m_b k_B T} / \hbar \gg 1$. Here n is the bath particle number density, $f(q, T)$ is the Boltzmann distribution at temperature T , and $\sigma(q)$ is the total scattering cross-section.

With an unscreened $1/r$ interaction, the above poses an immediate problem: the total cross section is infinite. This can be traced back to the long-range potential: the potential does not turn off sufficiently fast even as the bath particle moves arbitrarily far away, and the particle continues to scatter at infinitely late times [49].

The divergences associated with the $1/r$ potential occur even at the semiclassical level. For instance, a bath wavepacket far from the scattering center will continue, even neglecting any spread in the wavepacket about its mean location, to accumulate an overall phase

$$\phi(t) = \int^t dt' \frac{V_0}{|\mathbf{r} + \mathbf{v}t'|} \quad (44)$$

which grows without bound as $t \rightarrow \infty$. Above, the wavepacket is moving in a potential centered at the origin, \mathbf{r} is the initial location of the wavepacket, \mathbf{v} is its asymptotic velocity, V_0 is a coupling constant, and we are focusing on the behavior when $|\mathbf{v}t| \gg |\mathbf{r}|$.

However, in seeking to model the decohering effect of a distant bath particle upon a spatial superposition, there is a related quantity which remains finite, i.e. the difference of phases. A bath particle produces the relative phase shift between the two atom paths of the form

$$\Delta\phi \approx V_0 \int_0^t dt' \left(\frac{1}{|\mathbf{r}_1(t') - \mathbf{r} - \mathbf{v}t'|} - \frac{1}{|\mathbf{r}_2(t') - \mathbf{r} - \mathbf{v}t'|} \right). \quad (45)$$

Here, $\mathbf{r}_{1,2}$ represent the two locations of the atom along the superposition path, V_0 is a coupling constant, and \mathbf{r}, \mathbf{v} are, as in Eqn. 44, the initial position and velocity of the bath particle, respectively. At sufficiently long times $t \rightarrow \infty$ and assuming bounded r_1, r_2 , the late-time behavior of this integral is

$$\Delta\phi = V_0 \int^{t \rightarrow \infty} \frac{dt'}{|\mathbf{v}|^2 t'^2} < \infty \quad (46)$$

because the lowest-order terms, which would have diverged logarithmically, cancel. Thus there is no unregulated infrared divergence. This suggests that the resolution to the failure of naive collisional decoherence lies in carefully working in terms of regulated quantities, i.e. quantities defined in terms of the difference of the evolution between two paths.

To see how this shows up in the calculations already carried out, consider the following. If we followed the typical path integral method of calculation, the first thing to consider would be the phase associated with the potential difference between the two paths

$$\Delta\phi = \int (V(\mathbf{r}_1(t)) - V(\mathbf{r}_2(t))) dt \quad (47)$$

$$\approx \int dt \mathbf{F}(t) \cdot \Delta\mathbf{r}(t) \quad (48)$$

where $\mathbf{F} = -\nabla V$ and in the second line we assume that the force in the vicinity of the experiment is approximately constant in space. This of course is not accurate for bath particles close to the experiment, but the infrared divergence discussed above comes from the behavior of the interaction at large distances, so it is sufficient to study this case. Taking,

as in the protocol outlined above,

$$\Delta \mathbf{r}(t) = \begin{cases} kt/m_a \mathbf{e}_3 & t \in [0, \tau] \\ k(2\tau - t)/m_a \mathbf{e}_3 & t \in [\tau, 2\tau], \end{cases} \quad (49)$$

we have

$$\Delta\phi \approx \int_{\tau}^{2\tau} dt F_z(t)(k(2\tau - t)/m_a) + \int_0^{\tau} dt F_z(t)(kt/m_a) \quad (50)$$

$$= k \left(\int_0^{2\tau} \int_0^{t'} dt' dt'' \frac{F_z(t'')}{m_a} - 2 \int_0^{\tau} \int_0^{t'} dt' dt'' \frac{F_z(t'')}{m_a} \right) \quad (51)$$

$$\approx k(z(2\tau) - 2z(\tau)) \quad (52)$$

which is of course the semiclassical version of Eqn. 24 neglecting laser motion. We therefore stress that we evade divergences associated with the $1/r$ potential not simply because we model the bath classically (recall that divergence occurs even at the semiclassical level), but rather because we rigorously track *relative* evolution of the atomic superposition, in a way that will remain valid even beyond this lowest term in the semiclassical expansion of bath particle behavior. Our approach also goes beyond the infinite experimental mass limit of standard collisional decoherence, i.e. we account for how interaction with the bath warps the two paths of the interferometer. Finally, note that the finite result in Eqn. 46 suggests there is a scattering treatment of the problem one could consider applying in the case where the atom is held at two fixed locations for a long time, as in [50].

V. COLLISION CONE SECTOR

We now consider the effect of bath particles in the collision cone on atom interferometry signals. Recall that the collision cone consists of those background particles which at some point during the atom freefall come within the cutoff radius r_{min} . These particles come close to the setup in the sense that they source a potential which may vary significantly across the extent of the experiment. While closed form expressions for the scattering states of single particles in the Newton potential exist [49, 51], we use an approximation motivated by dark matter detection and focus on the impulse delivered by collision cone particles on the components of our interferometer.

Our approximation neglects self-consistent corrections that lead to high angle scattering. Specifically, in $1/r$ scattering, high angle scattering events correspond to substantial back-action on the incoming particle. We neglect the change in the motion of the bath particle to all orders, and keep the only the lowest order correction to changes in the motion of the interferometer. We also neglect quantum back-action, i.e. entanglement between the bath particle state and the atom state.

For simplicity we consider the effect of a single particle in the collision cone. In order to refer to the center of atomic motion more conveniently, we define

$$\mathbf{d} \equiv \mathbf{z}_0 + \frac{\hbar \mathbf{k} \tau}{2m_a}. \quad (53)$$

We use the impulsive limit to write down simple expressions for the force on the atom and the laser. Given the bath particle initial conditions we first calculate the times at which it comes nearest to the initial laser location $\mathbf{0}$ and the average atom location \mathbf{d} . This done, rather than write out the full expression for how the force changes continuously in time, we model it as instantaneous kicks delivered to the experimental components at the times of closest approach. With this model the force equations are

$$\dot{P}_{z, \text{laser}} = M_{\text{laser}} \delta v_z(\mathbf{0}) \delta(t - t_{\text{kick}}(\mathbf{0})) \quad (54)$$

$$\dot{\hat{p}}_z = m_a [\delta v_z(\mathbf{d}) + \nabla(\delta v_z(\mathbf{d})) \cdot (\hat{\mathbf{r}} - \mathbf{d}) + \mathcal{O}((\hat{\mathbf{r}} - \mathbf{d})^2)] \delta(t - t_{\text{kick}}(\mathbf{d})), \quad (55)$$

where $t_{\text{kick}}(\mathbf{r})$ is the time at which a bath particle with position \mathbf{r}_b and velocity \mathbf{v}_b at $t = 0$ comes closest to the point \mathbf{r}

$$t_{\text{kick}}(\mathbf{r}) \equiv -\frac{(\mathbf{r}_b - \mathbf{r}) \cdot \mathbf{v}_b}{v_b^2} \quad (56)$$

and the velocity kick function is defined by integrating the gravitational acceleration felt at \mathbf{r} over time

$$\delta v_z(\mathbf{r}) \equiv \int_{-\infty}^{\infty} dt \frac{G m_b (\mathbf{r}_b + \mathbf{v}_b t - \mathbf{r})}{|\mathbf{r}_b + \mathbf{v}_b t - \mathbf{r}|^3} = \frac{2 G m_b}{v_b} \frac{\left((\mathbf{r}_b - \mathbf{r}) + \mathbf{v}_b t_{\text{kick}}(\mathbf{r}) \right) \cdot \mathbf{e}_3}{\left((\mathbf{r}_b - \mathbf{r})^2 - v_b^2 t_{\text{kick}}^2(\mathbf{r}) \right)}. \quad (57)$$

Note the scaling $\delta v_z \propto Gm_b/v_b b$, where b is the impact parameter of the bath particle trajectory with respect to \mathbf{r} . The velocity kick function has gradient

$$\begin{aligned}\nabla(\delta v_z(\mathbf{r})) = & \frac{4Gm_b}{v_b} \frac{\left((\mathbf{r}_b - \mathbf{r}) + \mathbf{v}_b t_{\text{kick}}(\mathbf{r})\right) \cdot \mathbf{e}_3}{\left((\mathbf{r}_b - \mathbf{r})^2 - v_b^2 t_{\text{kick}}^2(\mathbf{r})\right)^2} \left((\mathbf{r}_b - \mathbf{r}) + \mathbf{v}_b t_{\text{kick}}(\mathbf{r})\right) \\ & - \frac{2Gm_b}{v_b} \frac{\mathbf{e}_3 - \mathbf{v}_b(\mathbf{v}_b \cdot \mathbf{e}_3)/v_b^2}{\left((\mathbf{r}_b - \mathbf{r})^2 - v_b^2 t_{\text{kick}}^2(\mathbf{r})\right)}.\end{aligned}\quad (58)$$

Because we assume that the bath particle still remains much farther than $k\tau/m_a$ from the atom at all times, the velocity kick felt by the atom at any point in its trajectory is well approximated by a linear correction to the velocity kick felt at \mathbf{d} . Going forward we will drop the terms beyond linear order in $\hat{\mathbf{r}} - \mathbf{d}$.

We can write down the evolution of the laser and atom positions

$$Z(t) = \Theta(t - t_{\text{kick}}(\mathbf{0})) (t - t_{\text{kick}}(\mathbf{0})) \delta v_z(\mathbf{0}) \quad (59)$$

$$\hat{z}(t) = \hat{z} + \frac{\hat{p}_z t}{m_a} + \Theta(t - t_{\text{kick}}(\mathbf{d})) (t - t_{\text{kick}}(\mathbf{d})) [\delta v_z(\mathbf{d}) + \nabla(\delta v_z(\mathbf{d})) \cdot (\hat{\mathbf{r}} + \frac{\hat{\mathbf{p}} t_{\text{kick}}(\mathbf{d})}{m_a} - \mathbf{d})] \quad (60)$$

where $\Theta(t)$ is the unit step function which results from integrating the delta function in time. The final overlap factor, which we use to determine the final ground state population according to Eqn. 19, is

$$\begin{aligned}\langle \mathbf{z}_0, 0 | (U^b)^\dagger U^t | \mathbf{z}_0, 0 \rangle = & e^{i\theta_0} \exp\{ik(\delta v_z(\mathbf{d})(\tau - |\tau - t_{\text{kick}}(\mathbf{d})|) - \delta v_z(\mathbf{0})(\tau - |\tau - t_{\text{kick}}(\mathbf{0})|))\} \\ & \times \exp\{i\frac{\hbar k^2}{2m_a} \partial_z(\delta v_z(\mathbf{d}))(t_{\text{kick}}(\mathbf{d}) - \tau)(\tau - |\tau - t_{\text{kick}}(\mathbf{d})|)\} \\ & \times \exp\{-\nabla(\delta v_z(\mathbf{d}))^2(\tau - |\tau - t_{\text{kick}}(\mathbf{d})|)^2(\frac{k^2 \sigma^2}{2} + \frac{\hbar^2 k^2 t_{\text{kick}}^2(\mathbf{d})}{8m_a^2 \sigma^2})\}.\end{aligned}\quad (61)$$

Let us examine the features of this expression. The first line gives a simple phase shift caused by relative motion of the atom and the laser. Note that a velocity kick to the laser system is just as easy to read out in the signal as a kick to the atom, which emphasizes that both components of the experiment contribute to its function as a sensor. The second term is a more complicated phase shift depending on the differential velocity kick to the two atom

paths. The third term gives an overall reduction in contrast since the differential velocity kicks to the two atom paths cause the different paths to end at slightly different positions and momenta, inhibiting their ability to interfere.

As the time of the velocity kicks approaches the beginning or end of the experiment $t_{\text{kick}}(\mathbf{0}), t_{\text{kick}}(\mathbf{d}) \rightarrow 0, 2\tau$, their effect disappears. To explain, at the beginning and end of the experiment the separation between atom paths is negligible and so the differential velocity kick is also negligible, while the relative motion of the laser and atom leads either to identical and therefore unobservable phase shifts on both arms ($t_{\text{kick}} \rightarrow 0$) or to negligible phase shifts ($t_{\text{kick}} \rightarrow 2\tau$). Notice that if the average kick to the atom equals the laser kick $\delta v_z(\mathbf{d}) = \delta v_z(\mathbf{0})$, and if these occur at the same time $t_{\text{kick}}(\mathbf{0}) = t_{\text{kick}}(\mathbf{d})$, then the phase shift resulting from relative motion between the atom and laser again disappears, but effects related to different velocity kicks on the two arms (set by $\nabla(\delta v_z)$, the velocity kick gradient) persist.

We now comment on prospects for observing this gravitational noise. The dominant contribution to Eqn. 61 is the phase shift in the first line whose characteristic size scales with experimental parameters like

$$\Delta\theta \approx k \delta v_z \tau. \quad (62)$$

Obviously, a measurement on a single atom is subject to shot noise and cannot give meaningful information on a small phase shift if the phase shift is not constant over many runs of the experiment. With N atoms in a single cloud, however, one reduces the shot noise by a factor of \sqrt{N} . The velocity sensitivity of the interferometer, then, scales like $(Qk\tau\sqrt{N})^{-1}$, where $\hbar k$ is the single photon momentum and Q is an integer to include the increased momentum kick of multiphoton transition pulses [52–56]. With reasonable experimental numbers the weakest observable kick, $\delta v_{z,\min}$ is roughly

$$\delta v_{z,\min} \approx 10^{-14} \frac{\text{m}}{\text{s}} \left(\frac{10^3}{Q} \right) \left(\frac{1}{k \times 780 \text{ nm}} \right) \left(\frac{1 \text{ s}}{\tau} \right) \left(\frac{10^6}{N} \right)^{1/2}. \quad (63)$$

For comparison, a heavy dark matter particle (with a mass of $100 m_{\text{pl}}$) passing within tens of meters of the atom produces a velocity kick on the order of 10^{-22} m/s . From the scaling of the velocity kick given just after Eqn. 57, $\delta v_z \propto b^{-1}$, we see that in order to produce a measurable phase shift the same dark matter particle would need to pass within hundreds of nanometers of the atom. An event of this type has negligible event rate and would of

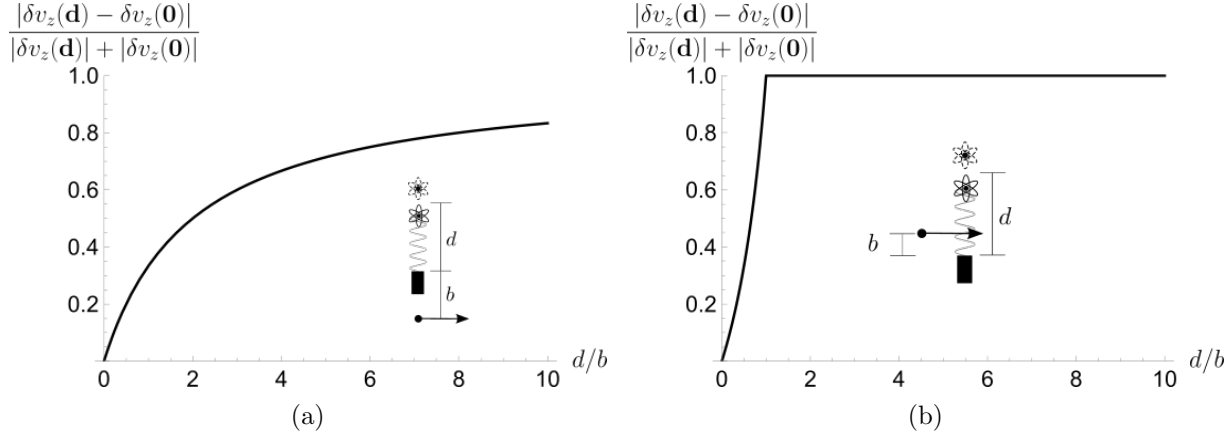


FIG. 3. Plot of the magnitude of the dominant phase shift in Eqn. 61 divided by the sum of the constituent phase shift magnitudes. For $d \ll b$ there is significant phase shift cancellation due to similar common motion of the laser and the atom. a) A bath particle passes below the laser. The size of the net phase shift is about 80% of the sum of the separate phase shift magnitudes for $d = 10b$, the ratio asymptotes to 1 in the limit $d/b \rightarrow \infty$. Increasing d far beyond b gives diminishing returns. b) A bath particle passes above the laser. The behavior resembles the previous case for $d/b \ll 1$, but as soon as $d > b$, the momentum kicks on the atom and laser are in opposite directions, so there is no common motion cancellation to the dominant phase shift.

course require calculations beyond the approximations we have made here to be analyzed.

VI. TUNING THE SENSOR: THE CHOICE OF ATOM-LASER DISTANCE

We now comment on the role of the tunable parameter $d \equiv z_0 + \hbar k \tau / 2m_a$, the distance between the laser and the center of atomic motion. In practice, the easiest way to adjust this is through z_0 , the initial atom-laser distance. Recognizing, as we have emphasized, that the laser system is part of the sensor, we now ask, what goes into optimizing the atom-laser distance for sensitivity to the gravitational background?

Recall that we found it useful to distinguish between two sectors of bath particle phase space, the distant sector and the collision cone. We will take these sectors in turn. In fact, however, the most significant change to effects from the distant sector when we change d is the redefinition of the distant sector itself. Physically, the atom-laser distance is important if one wants to see gravitational effects because it sets the cutoff beyond which effects of the bath have significant common motion cancellations. The notion of a distant sector therefore gets its meaning from the length scale d .

Mathematically, the dependence on d appears in the formula for decoherence resulting

from distant sector particles, Eqn. 41, both in an explicit factor of $d = z_0 + \hbar k \tau / 2m_a$ and implicitly in the characteristic size of gravitational field fluctuations $\xi^2 \propto 1/r_{min}^3$, through the condition $r_{min} \gg d$. Since r_{min} must scale up with d for the cutoff radius to contain the entire apparatus, the net effect is that contribution of distant sector particles to decoherence is diminished as the spatial extent of the experiment is increased. This makes intuitive sense. As we increase d , more and more particles we previously labeled as “distant” we now label as being in the collision cone. The decoherence from these particles still matters at large d , but is now attributed to the collision cone contribution.

The sensitivity of the interferometer to collision cone particles as we increase d is more interesting. The dominant contribution in the formula for the effect of collision cone particles, Eqn. 61, is a sum of the phase shift from the impulse on the laser and the phase shift from the mean impulse on the atom. Consider for simplicity a bath particle with velocity perpendicular to the z direction which passes through the point $(0, 0, -b)$ at time τ . Note that we focus on $-b < 0$ so that in the large d limit the dominant effect we need to analyze is the velocity kick to the laser. This is simpler to treat than the effect on the atomic superposition, but, as pointed out in the previous section, is still readily observable. Take the impact parameter b to be fixed, and consider changing the sensitivity of the signal to this bath particle by varying d . As shown in Fig. 3a, in the regime $d \ll b$, the magnitude of the net phase shift is much smaller than the sum of separate magnitudes of the laser shift and average atom shift (there is significant cancellation between the laser shift and atom shift), but as $d/b \rightarrow \infty$ the ratio of the two asymptotes to 1 (one of the shifts is much larger than the other). Over 80 % of the maximum recoverable phase shift is achieved when $d/b = 10$.

Very roughly, then, we can say that the signal is not significantly reduced by common motion cancellations for bath particles with impact parameter $\lesssim d$. A larger choice of d leads to greater sensitivity to particles with impact parameters on the order of the experiment size. However, since a larger impact parameter leads to weaker velocity kicks to the apparatus, at some point increasing d further “brings online” particles whose effect is too weak to be read out. Increasing d far beyond this length scale provides no advantage to the experiment. With the simplifications we have made in this section, the idea of a minimum velocity kick sensitivity from Eqn. 63 naturally leads to a maximum impact parameter b_{max} for bath particles in the collision cone such that their effect can be read out, i.e. the condition on d

such that the sensor not lose significant signal to common motion cancellations is

$$d \gg b_{max} \approx 1 \text{ nm} \left(\frac{m_b}{m_{pl}} \right) \left(\frac{10^{-14} \text{ m/s}}{\delta v_{z,\min}} \right). \quad (64)$$

There is no advantage to increasing d once it is already much larger than b_{max} , which we see above is automatically fulfilled in any realistic experiment. As a result, there is little practical significance in the choice of d .

VII. COSMIC RAYS

Finally, we consider the atom interferometer as a velocity kick detector for the case of bath particles coupled through electromagnetic forces. Note in this case, we do not need to track the evolution of the laser, which we take to be charge neutral and very massive. Consider a cosmic ray particle with charge q at location $\mathbf{r}_c(t)$. We neglect the many-electron internal structure of the atom, considering only a single valence electron and a nucleus of effective charge $+e$. Again, $\hat{\mathbf{r}}$ is the operator for the atomic center of mass. We also now need to consider $\hat{\mathbf{r}}'$, the relative coordinate operator, which gives the displacement of the electron from the nucleus. In the nonrelativistic limit, the interaction Hamiltonian of the atom with the cosmic ray particle is

$$\hat{H}' = \frac{qe}{4\pi\epsilon_0|\hat{\mathbf{r}} - \mathbf{r}_c|} - \frac{qe}{4\pi\epsilon_0|\hat{\mathbf{r}} + \hat{\mathbf{r}}' - \mathbf{r}_c|} \quad (65)$$

$$\approx -\frac{qe}{4\pi\epsilon_0|\hat{\mathbf{r}} - \mathbf{r}_c|^3} (\mathbf{r}_c - \hat{\mathbf{r}}) \cdot \hat{\mathbf{r}}' \quad (66)$$

$$= -\hat{\mathbf{d}} \cdot \mathbf{E}(\hat{\mathbf{r}}), \quad \hat{\mathbf{d}} \equiv -e\hat{\mathbf{r}}', \quad \mathbf{E}(\hat{\mathbf{r}}) \equiv -\frac{q}{4\pi\epsilon_0|\hat{\mathbf{r}} - \mathbf{r}_c|^3} (\mathbf{r}_c - \hat{\mathbf{r}}), \quad (67)$$

where to get the second line we assume that the distance of the cosmic ray from the atom is always much larger than the atom size. We then get a dipolar potential of the atom with the electric field produced by the cosmic ray.

We assume the cosmic ray passes far enough from atom that the electric field near the atom varies slowly in time and therefore we use the DC Stark effect to get in perturbation theory

$$\hat{H}' \approx -\frac{\alpha}{2} |E(\hat{\mathbf{r}})|^2 = -\frac{\alpha}{2} \frac{q^2}{(4\pi\epsilon_0)^2 |\hat{\mathbf{r}} - \mathbf{r}_c|^4}, \quad (68)$$

where α is the ground state polarizability. Note that now the energy depends only on the location of the atom center of mass.

The leading order effect for a cosmic ray particle much farther than the separation between atom paths is just the average velocity kick to the atom. This still produces a measurable phase shift because the atom moves relative to the laser. With impact parameter $\mathbf{b} \propto \mathbf{e}_3$ and a straight line charged particle trajectory we get

$$m_a \delta v_z \approx \alpha \left(\frac{q}{4\pi\epsilon_0} \right)^2 \int_{-\infty}^{\infty} dt \frac{1}{(\sqrt{b^2 + v^2 t^2})^5} \quad (69)$$

$$\delta v_z \approx \frac{\alpha}{m_a} \left(\frac{q}{4\pi\epsilon_0} \right)^2 \frac{1}{b^4 v}. \quad (70)$$

To get an order of magnitude estimate, we plug in c for the cosmic ray particle velocity, and take the atom to be rubidium, which has $\alpha_{\text{Rb}} \approx 4\pi\epsilon_0 \times 50 \text{ \AA}^3$ [57]. We consider a passing gold nucleus, $q = +79 e$. This gives

$$\delta v_z \approx 10^{-36} \frac{\text{m}}{\text{s}} \left(\frac{1 \text{ m}}{b} \right)^4. \quad (71)$$

In section V we say with typical experimental parameters one should be able to get a velocity kick sensitivity of roughly 10^{-14} m/s . We therefore need the cosmic ray particle to pass within about $3 \mu\text{m}$ of the atom to be able to read it out. This has a negligible event rate, and violates several of the assumptions in our calculation.

We can also consider boosting the interaction with an applied static field E_{applied} on the atom. This enhances the effect of cosmic ray particles with impact parameter parallel to the applied field. The size of the velocity kick now goes like

$$\delta v_z \approx \frac{\alpha}{m_{\text{Rb}}} \frac{e}{4\pi\epsilon_0 b^2} \left(E_{\text{applied}} + \frac{e}{4\pi\epsilon_0 b^2} \right) \frac{1}{v}. \quad (72)$$

Suppose we apply a static field on the order of 1 kV/m to the atom. The contribution from the cosmic ray particle gives a similar electric field at a distance of $1 \mu\text{m}$. From the numbers above, we see that even with the applied field, if the cosmic ray passes at a distance of $10 \mu\text{m}$, the phase shift is already undetectable (though suppressed only by a factor of 100 rather than 10^4 corresponding to the case without an applied field).

VIII. OUTLOOK

In this paper, we examined an explicit model for gravitational background noise in an atom interferometry experiment. By accounting for the effect of the noise on the control system in addition to the atom, we were able to illustrate how the equivalence principle suppresses the effect of bath particles far from the experiment. Clearly, it will be difficult to see such gravitational noise in any near term experiment.

IX. ACKNOWLEDGMENTS

We thank Gayathrini Premawardhana for helpful conversations and William McGehee and Eite Tiesinga for comments on the manuscript. DC is supported by the US Department of Energy under contract DE-AC02-05CH11231 and Quantum Information Science Enabled Discovery (QuantISED) for High Energy Physics grant KA2401032.

Appendix A: Time Dependence in the Distant Sector

When we include the time dependence of the bath, we get the following evolution of the relative displacement

$$\begin{aligned} \hat{z}(t) - Z_{\text{laser}}(t) \approx \hat{z} + t \frac{\hat{p}_z}{m_a} + G \int_0^t dt_1 \int_0^{t_1} dt_2 \Phi_j^z(t_2) \left(\hat{r}^j + t_2 \frac{\hat{p}^j}{m_a} \right) \\ + G^2 \int_0^t dt_1 \int_0^{t_1} dt_2 \Phi_j^z(t_2) \int_0^{t_2} dt_3 \int_0^{t_3} dt_4 \Phi_k^j(t_4) \left(\hat{r}^k + t_4 \frac{\hat{p}^k}{m_a} \right). \end{aligned} \quad (\text{A1})$$

Using the same initial atomic wavepacket $|\mathbf{z}_0, 0\rangle$ from in the main text we find

$$\begin{aligned}
\langle \mathbf{z}_0, 0 | (U^b)^\dagger U^t | \mathbf{z}_0, 0 \rangle = & e^{i\theta_0} \exp \left\{ ik \left(G \int^{2\tau} dt_1 \int^{t_1} dt_2 \left[\Phi_z^z(t_2)(z_0 + \frac{kt_2}{2m_a}) \right. \right. \right. \\
& \left. \left. \left. + \Phi_j^z(t_2)G \int^{t_2} dt_3 \int^{t_3} dt_4 \Phi_z^j(t_4)(z_0 + \frac{kt_4}{2m_a}) \right] \right. \right. \\
& \left. \left. - 2G \int^\tau dt_1 \int^{t_1} dt_2 \left[\Phi_z^z(t_2)(z_0 + \frac{kt_2}{2m_a}) \right. \right. \right. \\
& \left. \left. \left. + \Phi_j^z(t_2)G \int^{t_2} dt_3 \int^{t_3} dt_4 \Phi_z^j(t_4)(z_0 + \frac{kt_4}{2m_a}) \right] \right] \right\} \\
& \times \exp \left\{ - \left(G \int^{2\tau} \int^{t_1} dt_2 \Phi_j^z(t_2) - 2G \int^\tau \int^{t_1} dt_2 \Phi_j^z(t_2) \right)^2 \frac{k^2 \sigma^2}{2} \right. \\
& \left. - \left(G \int^{2\tau} \int^{t_1} dt_2 \Phi_j^z(t_2) t_2 - 2G \int^\tau \int^{t_1} dt_2 \Phi_j^z(t_2) t_2 \right)^2 \frac{k^2}{8m^2 \sigma^2} \right\}, \\
\end{aligned} \tag{A2}$$

$$\begin{aligned}
\langle \mathbf{z}_0, 0 | (U^b)^\dagger U^t | \mathbf{z}_0, 0 \rangle = & e^{i\theta_0} \exp \left\{ ik \left(G \int^{2\tau} dt_1 \int^{t_1} dt_2 \left[\Phi_z^z(t_2)(z_0 + \frac{kt_2}{2m_a}) + \Phi_j^z(t_2)G \int^{t_2} dt_3 \int^{t_3} dt_4 \Phi_z^j(t_4)(z_0 + \frac{kt_4}{2m_a}) \right] \right. \right. \\
& \left. \left. - 2G \int^\tau dt_1 \int^{t_1} dt_2 \left[\Phi_z^z(t_2)(z_0 + \frac{kt_2}{2m_a}) + \Phi_j^z(t_2)G \int^{t_2} dt_3 \int^{t_3} dt_4 \Phi_z^j(t_4)(z_0 + \frac{kt_4}{2m_a}) \right] \right] \right\} \\
& \times \exp \left\{ - \left(G \int^{2\tau} \int^{t_1} dt_2 \Phi_j^z(t_2) - 2G \int^\tau \int^{t_1} dt_2 \Phi_j^z(t_2) \right)^2 \frac{k^2 \sigma^2}{2} \right. \\
& \left. - \left(G \int^{2\tau} \int^{t_1} dt_2 \Phi_j^z(t_2) t_2 - 2G \int^\tau \int^{t_1} dt_2 \Phi_j^z(t_2) t_2 \right)^2 \frac{k^2}{8m^2 \sigma^2} \right\}, \\
\end{aligned} \tag{A4}$$

where a square over terms with one free index implies doubling and summing over the free index, i.e. $(\Phi_j^z + \dots)^2 \equiv \Phi_j^z \Phi_z^j + \dots$. In the main text we analyze the average over bath configurations of the phase shift in the above expression which is linear in Φ , as this term is responsible for the dominant effect in the static case. The dominant term \mathcal{D} from Eqn. 39 in the static case was made up of terms that are linear in Φ . In the case of time dependent Φ this becomes

$$\mathcal{D} = \exp \left\{ ikG \left(\int^{2\tau} dt_1 \int^{t_1} dt_2 \Phi_z^z(t_2)(z_0 + \frac{kt_2}{2m_a}) - 2 \int^\tau dt_1 \int^{t_1} dt_2 \Phi_z^z(t_2)(z_0 + \frac{kt_2}{2m_a}) \right) \right\}. \tag{A5}$$

Now we assume that we can approximate $\Phi_z^z(t_2)$ with a linear function in time,

$$\Phi_z^z(t) \approx \Phi_z^z(0) + \partial_t \Phi_z^z(t) \Big|_{t=0} t \quad (\text{A6})$$

where

$$\partial_t \Phi_z^z(t) \Big|_{t=0} = m_b \sum_{n=1}^N 3 \frac{(r_{b_n}^2 - 5z_{b_n}^2) \mathbf{r}_{b_n} \cdot \mathbf{v}_{b_n}}{r_{b_n}^7} + 6 \frac{z_{b_n} v_{z,b_n}}{r_{b_n}^5}. \quad (\text{A7})$$

This approximation assumes that we are looking at experimental runtimes still much shorter than the autocorrelation time of the bath. In particular, we assume $v_\beta \tau \ll r_{min}$. In this limit, we approximate the integral over the distant sector with an integral over all initial positions outside r_{min} and over all velocities regardless of initial position. As a result the correlation between $\Phi_z^z(0), \partial_t \Phi_z^z(0)$ vanishes by symmetry as $\partial_t \Phi_z^z(0)$ is linear in velocity, and we can treat the two quantities as independent Gaussian random variables, with

$$\langle (G \partial_t \Phi_z^z(0))^2 \rangle = \frac{48\pi}{5} \xi^2 \frac{v_\beta^2}{r_{min}^2}. \quad (\text{A8})$$

We can then straightforwardly extend the calculation from the static bath section to get

$$\langle \mathcal{D} \rangle_{Bath} = \exp\left\{-\frac{8\pi}{15} k^2 \left(z_0 + \frac{k\tau}{2m_a}\right)^2 \xi^2 \tau^4\right\} \exp\left\{-\frac{24\pi}{5} k^2 \left(z_0 + \frac{7}{12} \frac{k\tau}{m_a}\right)^2 \xi^2 \tau^4 \frac{v_\beta^2 \tau^2}{r_{min}^2}\right\}, \quad (\text{A9})$$

the lowest order correction in bath time dependence.

[1] A. D. Cronin, J. Schmiedmayer, and D. E. Pritchard, “Optics and interferometry with atoms and molecules,” *Rev. Mod. Phys.* **81**, 1051–1129 (2009).

[2] Pippa Storey and Claude Cohen-Tannoudji, “The Feynman path integral approach to atomic interferometry. A tutorial,” *J. Phys. II France* **4**, 1999–2027 (1994).

[3] M. O. Scully, B.-G. Englert, and H. Walther, “Quantum optical tests of complementarity,” *Nature* **351**, 111–116 (1991).

[4] G. Björk and A. Karlsson, “Complementarity and quantum erasure in welcher Weg experiments,” *Physical Review A* **58**, 3477–3483 (1998), publisher: American Physical Society.

[5] S. Dürr, T. Nonn, and G. Rempe, “Fringe Visibility and Which-Way Information in an Atom

Interferometer,” Physical Review Letters **81**, 5705–5709 (1998).

[6] S. Dürr and G. Rempe, “Complementarity and quantum erasure in an atom interferometer,” Optics Communications **179**, 323–335 (2000).

[7] K. Hornberger, S. Uttenthaler, B. Brezger, L. Hackermüller, M. Arndt, and A. Zeilinger, “Collisional decoherence observed in matter wave interferometry,” Phys. Rev. Lett. **90**, 160401 (2003).

[8] S. Dimopoulos, P. W. Graham, J. M. Hogan, and M. A. Kasevich, “General relativistic effects in atom interferometry,” Phys. Rev. D **78**, 042003 (2008).

[9] A. Peters, K. Y. Chung, and S. Chu, “High-precision gravity measurements using atom interferometry,” Metrologia **38**, 25–61 (2001).

[10] Z.-K. Hu, B.-L. Sun, X.-C. Duan, M.-K. Zhou, L.-L. Chen, S. Zhan, Q.-Z. Zhang, and J. Luo, “Demonstration of an ultrahigh-sensitivity atom-interferometry absolute gravimeter,” Phys. Rev. A **88**, 043610 (2013).

[11] C. Freier, M. Hauth, V. Schkolnik, B. Leykauf, M. Schilling, H. Wziontek, H.-G. Scherneck, J. Müller, and A. Peters, “Mobile quantum gravity sensor with unprecedented stability,” Journal of Physics: Conference Series **723**, 012050 (2016).

[12] J. M. McGuirk, G. T. Foster, J. B. Fixler, M. J. Snadden, and M. A. Kasevich, “Sensitive absolute-gravity gradiometry using atom interferometry,” Phys. Rev. A **65**, 033608 (2002).

[13] J. K. Stockton, K. Takase, and M. A. Kasevich, “Absolute geodetic rotation measurement using atom interferometry,” Phys. Rev. Lett. **107**, 133001 (2011).

[14] P. Asenbaum, C. Overstreet, T. Kovachy, D. D. Brown, J. M. Hogan, and M. A. Kasevich, “Phase shift in an atom interferometer due to spacetime curvature across its wave function,” Phys. Rev. Lett. **118**, 183602 (2017).

[15] J. M. Hogan *et al.*, “An atomic gravitational wave interferometric sensor in low earth orbit (AGIS-LEO),” General Relativity and Gravitation **43**, 1953–2009 (2011).

[16] P. W. Graham, D. E. Kaplan, J. Mardon, S. Rajendran, and W. A. Terrano, “Dark Matter Direct Detection with Accelerometers,” Phys. Rev. D **93**, 075029 (2016), arXiv:1512.06165 [hep-ph].

[17] B. Canuel *et al.*, “Exploring gravity with the MIGA large scale atom interferometer,” Scientific Reports **8**, 1–23 (2018).

[18] L. Badurina *et al.*, “AION: an atom interferometer observatory and network,” Journal of

Cosmology and Astroparticle Physics **2020**, 011–011 (2020).

[19] M. Abe *et al.*, “Matter-wave atomic gradiometer interferometric sensor (MAGIS-100),” (2021), arXiv:2104.02835 [physics.atom-ph].

[20] P. Hamilton, M. Jaffe, P. Haslinger, Q. Simmons, H. Müller, and J. Khoury, “Atom-interferometry constraints on dark energy,” *Science* **349**, 849–851 (2015).

[21] C. Burrage, E. J. Copeland, and E. Hinds, “Probing dark energy with atom interferometry,” *Journal of Cosmology and Astroparticle Physics* **2015**, 042 (2015).

[22] A. Peters, K. Y. Chung, and S. Chu, “High-precision gravity measurements using atom interferometry,” *Metrologia* **38**, 25 (2001).

[23] M. A. Fedderke, P. W. Graham, and S. Rajendran, “Gravity gradient noise from asteroids,” (2020), arXiv:2011.13833 [gr-qc].

[24] D. Carney, P. C. E. Stamp, and J. M. Taylor, “Tabletop experiments for quantum gravity: a user’s manual,” *Classical and Quantum Gravity* **36**, 034001 (2019).

[25] D. Carney, G. Krnjaic, D. C. Moore, C. A. Regal, G. Afek, S. Bhave, B. Brubaker, T. Corbitt, J. Cripe, N. Crisosto, A. Geraci, S. Ghosh, J. G. E. Harris, A. Hook, E. W. Kolb, J. Kun-jummen, R. F. Lang, T. Li, T. Lin, Z. Liu, J. Lykken, L. Magrini, J. Manley, N. Matsumoto, A. Monte, F. Monteiro, T. Purdy, C. J. Riedel, R. Singh, S. Singh, K. Sinha, J. M. Taylor, J. Qin, D. J. Wilson, and Y. Zhao, “Mechanical quantum sensing in the search for dark matter,” *Quantum Science and Technology* **6**, 024002 (2021), publisher: IOP Publishing.

[26] S. Bose, A. Mazumdar, G. W. Morley, H. Ulbricht, M. Toroš, M. Paternostro, A. A. Geraci, P. F. Barker, M. S. Kim, and G. Milburn, “Spin entanglement witness for quantum gravity,” *Phys. Rev. Lett.* **119**, 240401 (2017).

[27] M. Toroš, T. W. van de Kamp, R. J. Marshman, M. S. Kim, A. Mazumdar, and S. Bose, “Relative acceleration noise mitigation for entangling masses via quantum gravity,” (2020), arXiv:2007.15029 [gr-qc].

[28] S. Gerlich, S. Eibenberger, M. Tomandl, S. Nimmrichter, K. Hornberger, P. J. Fagan, J. Tüxen, M. Mayor, and M. Arndt, “Quantum interference of large organic molecules,” *Nature Communications* **2**, 263 (2011).

[29] J. Rodewald, N. Dörre, A. Grimaldi, P. Geyer, L. Felix, M. Mayor, A. Shayeghi, and M. Arndt, “Isotope-selective high-order interferometry with large organic molecules in free fall,” *New Journal of Physics* **20**, 033016 (2018).

[30] U. Delić, M. Reisenbauer, K. Dare, D. Grass, V. Vuletić, N. Kiesel, and M. Aspelmeyer, “Cooling of a levitated nanoparticle to the motional quantum ground state,” *Science* (2020).

[31] T. Westphal, H. Hepach, J. Pfaff, and M. Aspelmeyer, “Measurement of gravitational coupling between millimetre-sized masses,” *Nature* **591**, 225–228 (2021).

[32] T. Oniga and C. H.-T. Wang, “Quantum gravitational decoherence of light and matter,” *Phys. Rev. D* **93**, 044027 (2016).

[33] B. H. Pang, Y. Chen, and F. Y. Khalili, “Universal decoherence under gravity: A perspective through the equivalence principle,” *Phys. Rev. Lett.* **117**, 090401 (2016).

[34] I. Pikovski, M. Zych, F. Costa, and Č. Brukner, “Universal decoherence due to gravitational time dilation,” *Nature Physics* **11**, 668–672 (2015).

[35] A. Bassi, A. Großardt, and H. Ulbricht, “Gravitational decoherence,” *Classical and Quantum Gravity* **34**, 193002 (2017).

[36] C. Anastopoulos and B. L. Hu, “A master equation for gravitational decoherence: probing the textures of spacetime,” *Classical and Quantum Gravity* **30**, 165007 (2013).

[37] C. H.-T. Wang, R. Bingham, and J. T. Mendonça, “Quantum gravitational decoherence of matter waves,” *Classical and Quantum Gravity* **23**, L59–L65 (2006).

[38] S. Reynaud, P. A. M. Neto, A. Lambrecht, and M.-T. Jaekel, “Gravitational decoherence of planetary motions,” *Europhysics Letters (EPL)* **54**, 135–140 (2001).

[39] P. Kok and U. Yurtsever, “Gravitational decoherence,” *Phys. Rev. D* **68**, 085006 (2003).

[40] B. Lamine, M.-T. Jaekel, and S. Reynaud, “Gravitational decoherence of atomic interferometers,” *The European Physical Journal D - Atomic, Molecular, Optical and Plasma Physics* **20**, 165–176 (2002).

[41] M. R. Gallis and G. N. Fleming, “Environmental and spontaneous localization,” *Phys. Rev. A* **42**, 38–48 (1990).

[42] K. Hornberger and J. E. Sipe, “Collisional decoherence reexamined,” *Phys. Rev. A* **68**, 012105 (2003).

[43] S. L. Adler, “Normalization of collisional decoherence: squaring the delta function, and an independent cross-check,” *Journal of Physics A: Mathematical and General* **39**, 14067–14074 (2006).

[44] M.-T. Jaekel, B. Lamine, and S. Reynaud, “Phases and relativity in atomic gravimetry,” *Classical and Quantum Gravity* **30**, 065006 (2013).

- [45] S. Weinberg, “Infrared photons and gravitons,” *Phys. Rev.* **140**, B516–B524 (1965).
- [46] D. Carney, L. Chaurette, D. Neuenfeld, and G. W. Semenoff, “Infrared quantum information,” *Phys. Rev. Lett.* **119**, 180502 (2017), arXiv:1706.03782 [hep-th].
- [47] P. Storey and C. Cohen-Tannoudji, “The Feynman path integral approach to atomic interferometry. A tutorial,” *J. Phys. II France* **4**, 1999–2027 (1994).
- [48] W. P. Schleich, D. M. Greenberger, and E. M. Rasel, “A representation-free description of the Kasevich–Chu interferometer: a resolution of the redshift controversy,” *New Journal of Physics* **15**, 013007 (2013).
- [49] J. D. Dollard, “Asymptotic convergence and the coulomb interaction,” *Journal of Mathematical Physics* **5**, 729–738 (1964).
- [50] V. Xu, M. Jaffe, C. D. Panda, S. L. Kristensen, L. W. Clark, and H. Müller, “Probing gravity by holding atoms for 20 seconds,” *Science* **366**, 745–749 (2019).
- [51] I. W. Herbst, “On the connectedness structure of the Coulomb S -matrix,” *Communications in Mathematical Physics* **35**, 181–191 (1974).
- [52] T. Kovachy, P. Asenbaum, C. Overstreet, C. A. Donnelly, S. M. Dickerson, A. Sugarbaker, J. M. Hogan, and M. A. Kasevich, “Quantum superposition at the half-metre scale,” *Nature* **528**, 530–533 (2015).
- [53] S. M. Dickerson, J. M. Hogan, A. Sugarbaker, D. M. S. Johnson, and M. A. Kasevich, “Multiaxis inertial sensing with long-time point source atom interferometry,” *Phys. Rev. Lett.* **111**, 083001 (2013).
- [54] A. Miffre, M. Jacquey, M. Büchner, G. Tréneau, and J. Vigué, “Atom interferometry,” *Physica Scripta* **74**, C15–C23 (2006).
- [55] C. Overstreet, P. Asenbaum, and M. A. Kasevich, “Physically significant phase shifts in matter-wave interferometry,” *American Journal of Physics* **89**, 324–332 (2021).
- [56] S.-w. Chiow, T. Kovachy, H.-C. Chien, and M. A. Kasevich, “ $102\hbar k$ large area atom interferometers,” *Phys. Rev. Lett.* **107**, 130403 (2011).
- [57] M. D. Gregoire, I. Hromada, W. F. Holmgren, R. Trubko, and A. D. Cronin, “Measurements of the ground-state polarizabilities of Cs, Rb, and K using atom interferometry,” *Phys. Rev. A* **92**, 052513 (2015).